Monthly Notices
of the
ROYAL ASTRONOMICAL SOCIETY

MNRAS **449,** 1441–1448 (2015) doi:10.1093/mnras/stv348

Oxygen emission in remnants of thermonuclear supernovae as a probe for their progenitor system

D. Kosenko,[1⋆] W. Hillebrandt,[2] M. Kromer,[2,3] S. I. Blinnikov,[4,5,6] R. Pakmor[2,7] and J. S. Kaastra[8,9]

[1] *Sternberg Astronomical Institute (MSU), 119992, Universitetskij pr.13., Moscow, Russia*
[2] *Max-Planck-Institut für Astrophysik, Karl-Schwarzschild-Straße 1, D-85748 Garching, Germany*
[3] *The Oskar Klein Centre & Department of Astronomy, Stockholm University, AlbaNova, SE-106 91 Stockholm, Sweden*
[4] *Kurchatov Institute for Theoretical and Experimental Physics, Bolshaya Cheremushkinskaya 25, 117218 Moscow, Russia*
[5] *Kavli Institute for the Physics and Mathematics of the Universe (WPI), 5-1-5 Kashiwanoha, Kashiwa, Chiba 277-8583, Japan*
[6] *VNIIA, Moscow 127055, Russia*
[7] *Heidelberger Institut für Theoretische Studien, Schloss-Wolfsbrunnenweg 35, D-69118 Heidelberg, Germany*
[8] *SRON Netherlands Institute for Space Research, Sorbonnelaan 2, NL-3584 CA Utrecht, the Netherlands*
[9] *Leiden Observatory, Leiden University, PO Box 9513, NL-2300 RA Leiden, the Netherlands*

Accepted 2015 February 17. Received 2015 February 8; in original form 2014 October 11

ABSTRACT

Recent progress in numerical simulations of thermonuclear supernova explosions brings up a unique opportunity in studying the progenitors of Type Ia supernovae. Coupling state-of-the-art explosion models with detailed hydrodynamical simulations of the supernova remnant evolution and the most up-to-date atomic data for X-ray emission calculations makes it possible to create realistic synthetic X-ray spectra for the supernova remnant phase. Comparing such spectra with high-quality observations of supernova remnants could allow us to constrain the explosion mechanism and the progenitor of the supernova. The present study focuses in particular on the oxygen emission line properties in young supernova remnants, since different explosion scenarios predict a different amount and distribution of this element. Analysis of the soft X-ray spectra from supernova remnants in the Large Magellanic Cloud and confrontation with remnant models for different explosion scenarios suggest that SNR 0509−67.5 could originate from a delayed detonation explosion and SNR 0519−69.0 from an oxygen-rich merger.

Key words: hydrodynamics – ISM: supernova remnants – supernovae: individual: 0509−67.5 – supernovae: individual: 0519−69.0.

1 INTRODUCTION

There is general consensus that SNe Ia are exploding white dwarfs (WDs), composed of carbon and oxygen, where the explosion is triggered by mass transfer from a companion star (e.g. Hillebrandt & Niemeyer 2000). Traditionally, two classes of potential binary progenitor systems are distinguished: the single-degenerate progenitor channel (SD), in which the companion of the WD is a normal star (Whelan & Iben 1973), and the double-degenerate channel (DD) with two WDs interacting and merging (Iben & Tutukov 1984). At present it is unclear whether one of these possibilities is exclusively realized in nature or whether both contribute to the class of SNe Ia. In the past, it was believed that in the SD scenario the exploding WD has to be close to the Chandrasekhar-mass limit to ignite explosive carbon burning, first as a subsonic combustion wave (deflagration) with a likely transition to a detonation after it has expanded to somewhat lower density, in order to be in agreement with the observed light curves and spectra. The major disadvantage of this scenario was too low a number of events predicted by binary population synthesis. The DD scenario, on the other hand, had the disadvantage that theory predicted that the process of merging would lead to an accretion-induced collapse rather than a thermonuclear disruption (see Hillebrandt & Niemeyer 2000, for a review).

More recently, supported by increasing evidence from observations, the picture has emerged that SNe Ia are a more diverse class of objects (Li et al. 2011). The SD channel now includes WDs that explode with a mass significantly below the Chandrasekhar mass, the explosion being triggered by the detonation of a layer of helium on top, accreted from the companion, the so-called ‘sub-Chandrasekhar double-detonation’ scenario (Livne

⋆ E-mail: daria.kosenko@gmail.com

1990; Fink, Hillebrandt & Röpke 2007; Moll & Woosley 2013). In fact, this scenario is not limited to the SD channel. It may happen that during the process of merging helium from the outer layers of the companion WD is accreted on to the primary and burns explosively there (Pakmor et al. 2013). In addition, the DD channel may include binaries with a He WD as secondary companion instead (see Hillebrandt et al. 2013, for a recent review).

For our present study it is important that the various explosion scenarios yield element abundances and distributions which can be rather different and can, in principle, be distinguished by observations. For instance, Chandrasekhar-mass delayed-detonation models and the sub-Chandrasekhar ones predict generic differences for the iron-group elements because, in the first scenario, subsonic turbulent nuclear burning at high density goes together with convective mixing (Seitenzahl et al. 2013), whereas in the second scenario the density at ignition, set by the WD's mass, determines the final abundances and their distribution, and there is no mixing (Shigeyama et al. 1992; Sim et al. 2010). Some DD mergers, on the other hand, may have iron-group abundances very similar to the SD sub-Chandrasekhar explosions if the secondary WD is left behind unburned.

As far as lighter elements, such as oxygen, are concerned significant differences exist between the various scenarios as well. In DD mergers with a CO WD companion there may be a lot of unburned oxygen in the system, by default a generic feature of models in which the secondary is disrupted but not completely burned (Pakmor et al. 2012). In contrast, delayed-detonation Chandrasekhar-mass models have little oxygen, but at high velocity (Seitenzahl et al. 2013), as have accreting sub-Chandrasekhar models (Fink et al. 2010). In pure-deflagration Chandrasekhar-mass models, finally, due to mixing, low-velocity oxygen could also be present (Fink et al. 2014). It is the main goal of this paper to investigate if such differences may leave signatures in the X-ray emission during the supernova's remnant phase.

In a supernova remnant (SNR) when the reverse shock propagates inwards into the SN ejecta, the heated ejecta start to produce thermal X-ray emission, whose properties are determined by the chemical composition of the plasma (see Vink 2012, for a review). We perform numerical hydrodynamical simulations of an SNR evolution for different thermonuclear explosion scenarios. The analysis of the synthetic soft X-ray spectra built from these hydrodynamical models shows that the properties of the respective oxygen emission lines systematically vary from model to model.

To assess the significance of these variations we confront the numerical models with observations of young SNRs located in the Large Magellanic Cloud (LMC), SNR 0509−67.5 and SNR 0519−69.0. To estimate the oxygen contribution to the emission, we use data from the reflective grating spectrometer (RGS) on board the *XMM–Newton* observatory. We consider these objects as good case studies as the available high-resolution soft X-ray spectra clearly show the presence of bright oxygen emission lines (Kosenko et al. 2008; Kosenko, Helder & Vink 2010). Moreover, these objects are fairly well studied, so estimates of their dynamical properties (such as size, age and ISM density) are available in the literature.

The structure of the paper is as follows. We outline the explosion models used in this study in Section 2 and describe our method in Section 3. Results from our simulations and the corresponding synthetic X-ray spectra are discussed in Section 4. A detailed description of two LMC remnants and an analysis of the oxygen lines in their spectra are presented in Section 5. A comparison of our models with the observed data is given in Section 6. Finally, we discuss our results in Section 7 and conclude in Section 8.

2 EXPLOSION MODELS

For the present study we have picked three hydrodynamical models which may be considered as being 'typical' for some of the explosion scenarios introduced in Section 1, and for explaining 'normal' SNe Ia. The models were chosen to produce about 0.6 $M_\odot$ of ^{56}Ni in all cases such that the predicted luminosity at peak would agree with 'normal' SNe Ia.

The first model ('subch', 1.1 $\times 10^{51}$ erg) is from the class 'sub-Chandrasekhar double detonations' as described in Fink et al. (2010) and Sim et al. (2010). In the work of Fink et al. (2010) the core detonation is caused by the detonation of a thin He shell of a few 10^{-2} $M_\odot$. In contrast, in the Sim et al. (2010) work the CO core detonation is an assumption and the effect of the He layer on light curve and spectra is ignored, the goal being to study the general behaviour of such models rather than detailed spectra. The particular model we use here is not described in those papers but was chosen to match the radioactive Ni mass of the other two models discussed below. It consists of a bare 1.1 $M_\odot$ CO WD with an artificially ignited central detonation. After explosion, the simulation yields 0.615 $M_\odot$ of ^{56}Ni and the mass of oxygen is 0.07 $M_\odot$, with velocities from about 14 000 to more than 25 000 km s^{-1}. Synthetic light curve and spectra resemble normal SNe Ia rather well.

The second model ('deldet'; 1.4 $\times$ 10^{51} erg) is a 'classical' delayed-detonation model (Röpke et al. 2012; Seitenzahl et al. 2013). In this model, a Chandrasekhar-mass WD was set up in hydrostatic equilibrium with a central density of 2.9 $\times$ 10^9 g cm^{-3} and an electron fraction of $Y_e = 0.498\,864$, corresponding to solar metallicity. An initial deflagration was ignited in 100 sparks placed randomly in a Gaussian distribution within a radius of 150 km from the WD's centre in order to get approximately 0.6 $M_\odot$ of ^{56}Ni. After an initial deflagration phase a detonation was triggered based on the strength of turbulent velocity fluctuations at the flame front (for details on the treatment of the deflagration-to-detonation transition, see Ciaraldi-Schoolmann, Seitenzahl & Röpke 2013). The evolution was followed to a time of 100 s after ignition, by which homologous expansion of the ejecta was reached to a good approximation. This model fits the data of SN 2011fe in M101 reasonably well (Röpke et al. 2012). The mass of oxygen predicted by the model is 0.101 $M_\odot$, slightly above the sub-Chandrasekhar model presented here. Typical oxygen velocities are in the range from 10 000 to 20 000 km s^{-1}.

The third model ('merger', 1.6 $\times$ 10^{51} erg) we will use for our comparison with X-ray data is the inspiral, merger, and explosion of two CO WDs with 1.1 $M_\odot$ and 0.9 $M_\odot$, respectively. Details of the corresponding simulations are given by Pakmor et al. (2012). In this simulation, the inspiral and merger phases were followed with a version of the SPH code GADGET (Springel 2005) and the subsequent thermonuclear detonation was modelled with techniques similar to those employed in the delayed-detonation model described before. The question of whether a detonation triggers at the interface between the two merging stars is controversial. In our simulations we assumed a detonation to trigger when in one location the temperature exceeded 2.5 $\times$ 10^9 K in material of $\rho \approx 2 \times 10^6$ g cm^{-3} (Seitenzahl et al. 2009). Again, the evolution was followed up to 100 s and the composition of the ejecta was determined in a post-processing step. Also this model was used for a comparison with SN 2011fe by Röpke et al. (2012). Here the oxygen mass in the ejecta is considerably higher than in the two other models, namely 0.492 $M_\odot$ and the abundance distribution, in particular that of the iron-group elements is far less symmetric. Typical oxygen velocities range from a few 1000 to 20 000 km s^{-1}.

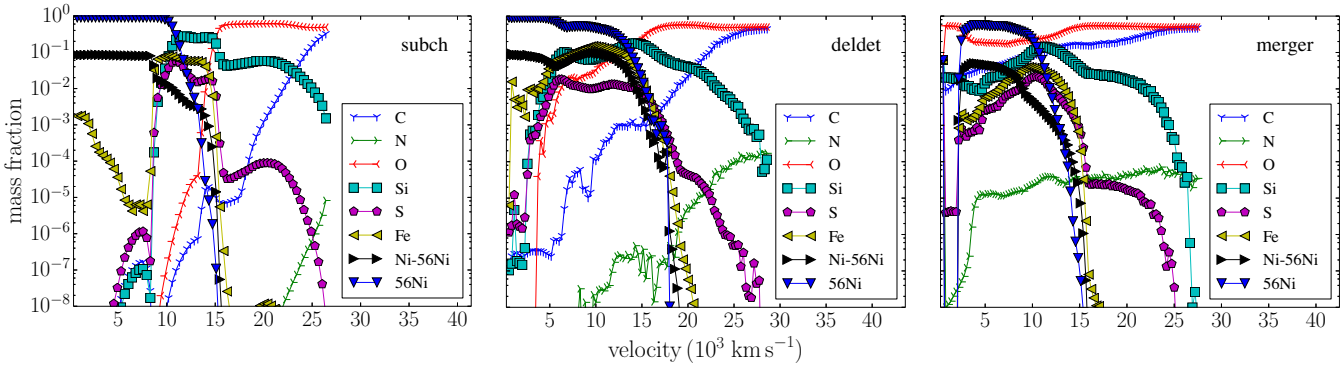

Figure 1. Spherically averaged radial abundance profiles of the most prominent elements as functions of ejecta velocity. The model's age is 10 yr.

For all three models the element abundances and their distribution differ (Fig. 1) which will become important when we discuss their X-ray spectra.

3 METHOD

For our hydrodynamical (HD) simulations of the SNR evolution we apply the SUPREMNA code (Blinnikov et al. 1998; Sorokina et al. 2004; Kosenko 2006). SUPREMNA uses an implicit Lagrangian formulation and takes into account the most important relevant physical processes, such as electron thermal conduction and a self-consistent calculation of the time-dependent ionization of the shocked plasma. The contribution of relativistic cosmic ray particles to the dynamics is treated in a two-fluid approximation (Kosenko, Blinnikov & Vink 2011). Since SUPREMNA assumes spherically symmetric ejecta, we use spherically averaged versions of the multi-dimensional explosion models described above, keeping in mind that there could be complications for the 'merger' model.

The HD package is coupled with the most up-to-date atomic data from the SPEX spectral fitting software (Kaastra, Mewe & Nieuwenhuijzen 1996) to obtain synthetic X-ray spectra from the modelled SNR. The call of the SPEX routine is executed for each cell of the HD grid. The total spectra are obtained by integrating over the entire model.

4 NUMERICAL SIMULATIONS

The SNR evolution was modelled for each of the three explosion scenarios. We start the simulations at a time of ∼3 years after the explosion (the explosion models were expanded accordingly with the unstable nickel decayed to iron). The remnants expand through a uniform interstellar medium (ISM) with a temperature of 10^4 K and various densities n_0. We set the ratio of electron to ion temperature to 0.3. Electron thermal conduction was suppressed (Sorokina et al. 2004) and diffusive shock acceleration (DSA) processes were neglected. However, we run one model with a moderate DSA efficiency in order to estimate its impact on the final results.

To illustrate how the composition of the models influences the emission from remnants, synthetic X-ray spectra in the range of (0.45–0.7) keV at a remnant's age of ∼430 yr are presented in Fig. 2. The spectra are shown for different values of n_0 (marked in the middle column). The lines of O VII at 0.57 keV, O VIII at 0.65 keV, and N VII and N VI at 0.5 keV (marked in the middle row) are visible for all models and ISM densities.

The spectra in Fig. 2 reveal that in the 'subch' and 'deldet' models most of the carbon is depleted, while the 'merger' is rich in the light elements. In the 'subch' and 'deldet' models the ejecta C VI contribution at 0.46 keV is absent, and only the S XIII complex at 0.47 keV is noticeable for $n_0 \gtrsim 1.0\,\mathrm{cm}^{-3}$. In the 'merger' spectra the sulphur contribution cannot be distinguished as it mixes with the relatively bright carbon line seen as an emission excess at 0.45–0.49 keV.

5 ANALYSIS OF THE OXYGEN EMISSION LINES FOR THE VARIOUS EXPLOSIONS

To estimate the line brightness, we consider the flux (F_X) of a line and its equivalent width, EW $= \int (F_X - F_0)\,\mathrm{d}E / \int F_0\,\mathrm{d}E$, where F_0 is the continuum flux at the line centroid. Furthermore, we calculate ratios of the oxygen emission line characteristics relative to those of nitrogen. Although the 'merger' model yields noticeable amount of nitrogen (mass fraction of $\sim 3 \times 10^{-5}$), it is still negligible compared to the solar abundance of $\sim 10^{-3}$ and to the nitrogen fraction in the LMC, which we assume is approximately a factor of 3 less than that of the Milky Way (e.g. Welty et al. 1999; Piatti & Geisler 2013). By relating the ejecta emission to the emission from the shocked ISM, we partially eliminate the effects of the unknown properties of the underlying continuum.

The EW is a measure of the total amount of the emitting particles. It takes into account all the particles with different velocities, thus accounting for the effects of the Doppler broadening. However, the EW depends on the continuum level around the line, which includes thermal and non-thermal components and depends on unknown plasma parameters (ion and electron temperatures, density, filling factor, etc.). In addition, our 1D hydrodynamical method cannot predict the X-ray continuum with sufficient accuracy.

Using the ratios of the line fluxes alleviates the influence of the continuum but does not account for the Doppler effect. However, we expect the line velocity broadening of the shocked oxygen in the ejecta and of the shocked nitrogen in the ISM to be correlated. A time evolution of the dimensionless EWs of O VII/N VII (solid) and O VIII/N VII (dashed) for our models and different ISM densities is presented in Fig. 3.

The time when the profiles reach their maximum is determined by the energy of the respective explosion. The amplitude of the EW ratios depends on the amount of oxygen. In remnants younger than 100–200 yr the ISM nitrogen line is rather weak, which explains the high values of the EW ratios at this stage. At an age of several hundred years the nitrogen line becomes pronounced and the respective EW ratios drop.

At low ISM densities and early times of $\lesssim 100$ yr (the left plot of Fig. 3) the 'deldet' and 'merger' profiles both produce weak

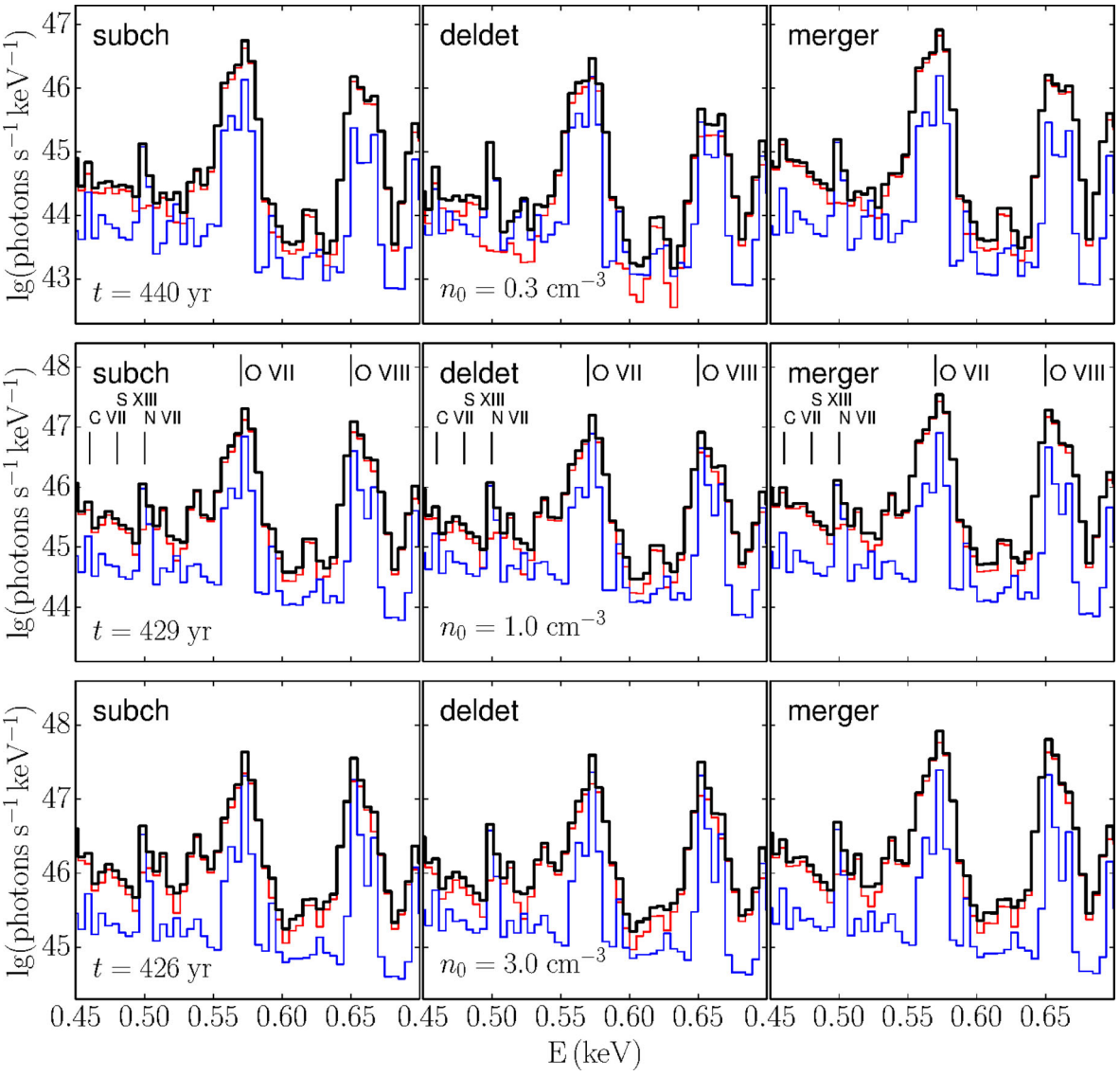

Figure 2. Synthetic X-ray spectra for different ambient medium densities. S XV is at 0.45 keV, C VI line is at 0.46 keV, S XIII is at 0.46–0.47 keV, N VII line is at 0.5 keV, O VII is at 0.57 keV, and O VIII is at 0.65 keV (marked in the middle row). Blue thin lines are for the shocked ISM, thin red for the shocked ejecta, thick black line is the total emission. The exact time of the model is in the left column, and the ISM density is indicated in the middle column.

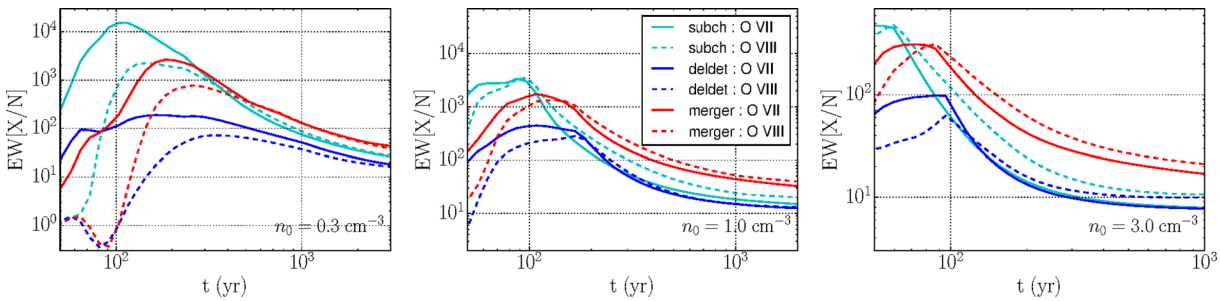

Figure 3. Evolution of the equivalent width ratios of O VII/N VII (solid) and O VIII/N VII (dashed) for different ambient densities ($n_0 = 0.3, 1.0, 3.0\,\mathrm{cm}^{-3}$ from left to right, respectively).

oxygen emission relative to nitrogen. Different oxygen abundance is balanced by the different explosion energy, so that the normalized oxygen emissivity is comparable. However, later (e.g. starting from 100 yr for the left plot with $n_0 = 0.3\,\mathrm{cm}^{-3}$) the 'merger' scenario yields higher oxygen emissivity.

For the high-density models the 'merger' profiles clearly stand out compared to the other two cases. The profiles for the 'deldet' model are lower, as this scenario has almost as much oxygen as the 'subch' model while it is almost as energetic as the 'merger' model. High-velocity outer layers of the ejecta lead to the expansion

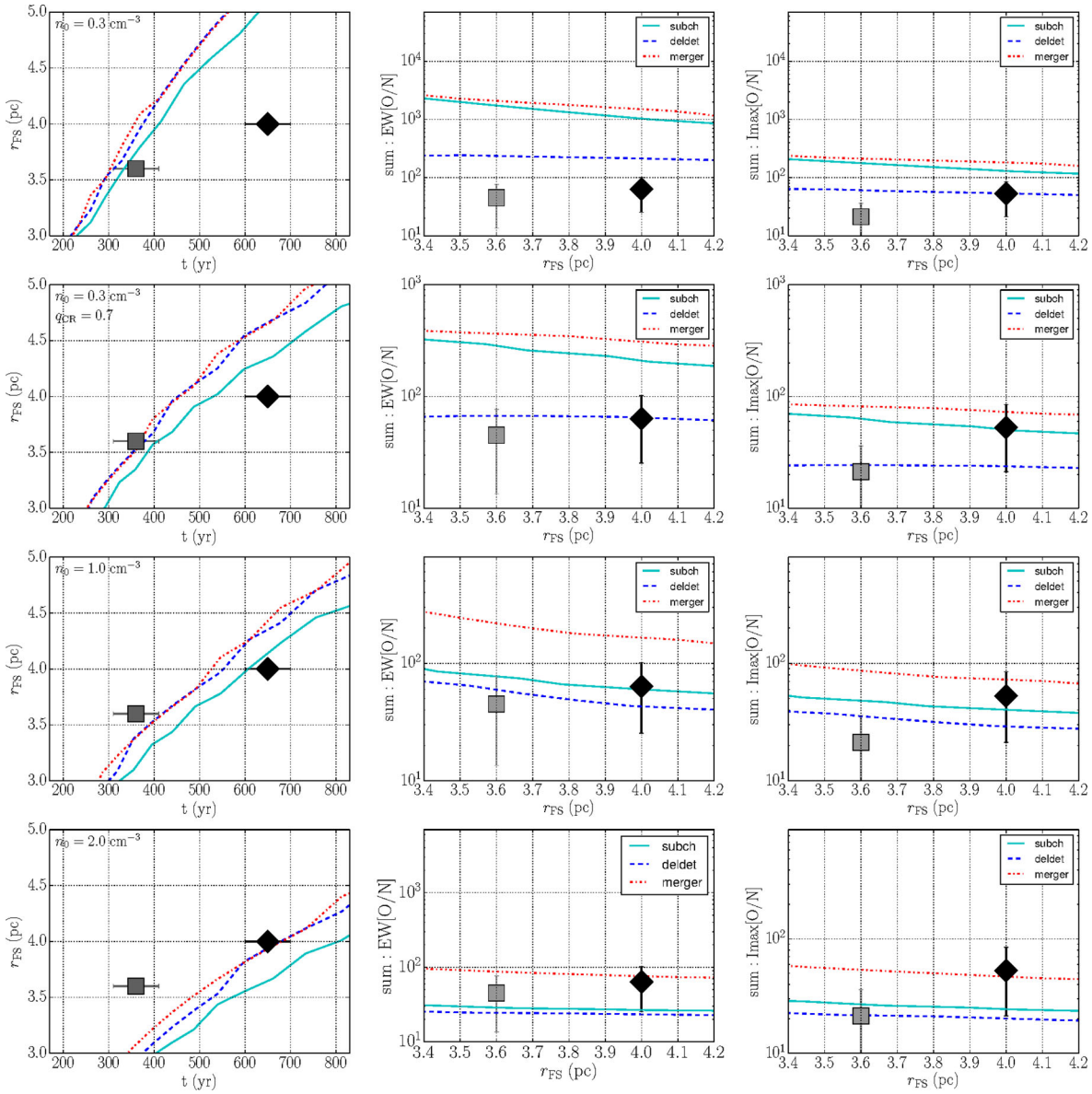

Figure 4. Left column: FS radii as a function of time for different explosion models (as indicated by the legends in the middle and right columns). Middle/right column: evolution of the oxygen to nitrogen EW and flux ratios, respectively. The evolution of the different models is mapped against the corresponding FS radius. Squared markers correspond to the measurements of SNR 0509−67.5 and diamonds to SNR 0519−69.0. Horizontal error bars are the age uncertainty as estimated in Kosenko, Ferrand & Decourchelle (2014). Vertical error bars are derived from the data 1σ uncertainty of nitrogen flux/EW measurements. The different rows correspond to different ISM densities as indicated in the labels in the left column. The simulations in the second row account for DSA by cosmic rays (acceleration parameter $q_{CR} = 0.7$).

of the forward shock (FS) as fast as in the 'merger' model (see the dynamics in the left column plots of Fig. 4) involving more nitrogen from the ambient medium, which reduces the respective normalized EW. Thus, relatively weak oxygen lines are normalized by the relatively bright nitrogen emission. At higher densities/later times (right panel of Fig. 3), when the reverse shock takes over the inner layers of the ejecta, the oxygen emissivity of the 'subch' and 'deldet' models decreases more rapidly compared to the 'merger'. This is a consequence of the different oxygen distribution in the inner layers of the explosion models.

A few HD evolutionary models taking into account DSA were also created. The modified models were built for $n_0 = 0.3\,\mathrm{cm}^{-3}$ and an acceleration parameter $q_{CR} \equiv P_{CR}/P_{tot} = 0.7$, where P_{CR} and P_{tot} are the cosmic ray and the total pressure at the FS, respectively (developed by Kosenko et al. 2011). For demonstration purposes this parameter was chosen higher than typical expected values of q_{CR} for SNRs; e.g. for Tycho SNR Kosenko et al. (2011) found $q_{CR} \simeq 0.5$–0.7 (in the assumption of constant cosmic ray diffusion coefficient).

6 OXYGEN IN SUPERNOVA REMNANTS IN THE LARGE MAGELLANIC CLOUD

To determine whether the difference in the oxygen emission line properties can in principle be detected in SNR spectra, we considered *XMM–Newton* observations of two young remnants in the LMC: SNR 0509−67.5 (OBSID 0111130201) and SNR 0519−69.0 (OBSID 0113000501). We analysed their RGS (den Herder et al.

2001) data using the standard method described in the *XMM–Newton* ABC Guide (cleaned for soft protons and subtracted the background).

The spectra in the range of (0.45–0.7) keV were fitted with a power law and four Gaussians for the four lines of interest (C VI, N VII, O VII, and O VIII with the XSPEC[1] software package; Arnaud 1996). The flux ratios were calculated as the ratios of the respective normalizations; the EW values are provided by the EQWIDTH utility applied to each Gaussian component.

Due to the poor data statistics, we did not apply the Galactic foreground absorptions in these fits. This simplification is acceptable because we do not use absolute values of fluxes. The best-fitting photon index for SNR 0509−67.5 is $\sim$3.8 $\pm$ 0.4 and for SNR 0519−69.0 is 0.7 $\pm$ 0.2. These measurements are in agreement with the low column density ($n_{\rm H}$ $<10^{21}$ cm^{-2}) found in Warren & Hughes (2004) in the SNR 0509−67.5 direction. In addition, spectral fitting of Kosenko et al. (2008) shows no evidence of the Galactic interstellar absorption for this SNR. For SNR 0519−69.0, however, Kosenko et al. (2010) reported $n_{\rm H} \simeq 2.6\times 10^{21}$ cm^{-2}.

Even though the χ^2/d.o.f. values of the fits are satisfactory (0.99 for SNR 0509−67.5 and 0.98 for SNR 0519−69.0), the quality of the data does not allow us to estimate the parameters of the lines with adequate precision. The relative errors of the weak nitrogen line are rather large, reaching $\sim$70 per cent (1σ). Thus, the derived fluxes and EWs should be used with caution and may serve only as approximate indications.

In order to confront the data with the models it is essential to know the dynamical properties and evolutionary stages of the remnants with sufficient accuracy. The analysis of SNR 0509−67.5 data reported by Kosenko et al. (2008) gives an ISM density of $n_0 = (0.4–0.6)\,{\rm cm}^{-3}$, Warren & Hughes (2004) measured $n_0 = 0.05\,{\rm cm}^{-3}$, and an SNR parametric analysis reported in Kosenko et al. (2014) constrains n_0 to $(0.1–0.3)\,{\rm cm}^{-3}$ (for an SN explosion of 10^{51} erg). Using light echo measurements Rest et al. (2005) limited the age of SNR 0509−67.5 to 400 $\pm$ 120 yr. Measurements of Ghavamian et al. (2007) give an age in the range 300–600 yr. Badenes et al. (2008) suggested that the remnant originated 400 years ago and expands through an ISM with $0.4\,{\rm cm}^{-3}$. They confirmed the results of Rest et al. (2008) where it was found that the SNR originated from an explosion similar to SN 1991T, releasing an energy of 1.4×10^{51} erg and producing almost one solar mass of ^{56}Ni.

The *XMM Newton* X-ray data from SNR 0519−69.0 studied by Kosenko et al. (2010) provide an ISM density estimate of $(2.4 \pm 0.2)\,{\rm cm}^{-3}$ and $\sim$0.4 M$_\odot$ of oxygen in the shocked ejecta. Note that the oxygen abundance derived from the spectral fitting is about four times higher than in SNR 0509−67.5. The parametric studies (Kosenko et al. 2014) give $n_0 = (0.5–1.0)\,{\rm cm}^{-3}$ (for an explosion energy of 10^{51} erg) and the light echo measurements of Rest et al. (2005) indicate an age of 600 $\pm$ 200 yr.

Even though in Kosenko et al. (2014) the ages for SNR 0509−67.5 and SNR 0519−69.0 were constrained to 310–410 yr and 600–700 yr, respectively, these spans are still too wide to identify the dynamical stages of these remnants. On the other hand, their angular dimensions are measured with relatively high accuracy due to the known distance to the LMC. Warren & Hughes (2004) reported a radius of 3.6 pc for the shell of SNR 0509−67.5 and the radius of the FS in SNR 0519−69.0 is 4.0 pc (Kosenko et al. 2010). Thus, in Fig. 4 we show the evolution of the [O VII+O VIII]/[N VII] ratios of the EWs and fluxes mapped against the corresponding radius instead of the remnant's age (the middle and the right columns). The HD SNR evolutionary models[2] numerically computed by SUPREMNA for ISM densities of $n_0 = 0.3\,{\rm cm}^{-3}$, $n_0 = 0.3\,{\rm cm}^{-3}$ with DSA, $n_0 = 1.0\,{\rm cm}^{-3}$, and $n_0 = 2.0\,{\rm cm}^{-3}$ are depicted in the left columns of Fig. 4. The squares and the diamonds correspond to the measurements of SNR 0509−67.5 and SNR 0519−69.0 correspondingly.

The dynamical evolution profiles (left column) and the data show that for SNR 0509−67.5 the acceptable ISM density lies approximately in the range of $(0.2–0.7)\,{\rm cm}^{-3}$ for the 'subch' model and of $(0.3–1.0)\,{\rm cm}^{-3}$ for the 'deldet' and 'merger' models. This implies that for these ranges of the ISM density in our set up the dynamics of SNR 0509−67.5 matches the dynamics of the corresponding models. The range for the 'subch' model is not explored by Fig. 4 and can be estimated from either linear interpolation between $0.3\,{\rm cm}^{-3}$ − 330 yr and $1.0\,{\rm cm}^{-3}$ − 470 yr or adopting locally Sedov ($n_0 \propto t^2$) expansion in the vicinity of $0.3\,{\rm cm}^{-3}$ $\propto$ 330 yr and $1.0\,{\rm cm}^{-3}$ $\propto$ 470 yr.

On the other hand, the oxygen emission profiles (in the middle and the right columns) exclude our 'subch' model for $n_0 \lesssim 0.5$ (for simplicity no DSA assumed). In contrast, our 'deldet' model matches the oxygen emissivity of SNR 0509−67.5 in the required dynamics range of $n_0 = (0.3–1.0)\,{\rm cm}^{-3}$. However, keep in mind that CR acceleration will change these estimates towards slightly lower values of n_0.

For SNR 0519−69.0 the dynamical evolution requires $n_0 \simeq (0.8–1.5)\,{\rm cm}^{-3}$ for the 'subch' model, and $n_0 \simeq (1.5–2.5)\,{\rm cm}^{-3}$ for the 'deldet' and 'merger' models. Even though the available precision of the oxygen emission data does not exclude the 'subch' model for this remnant, the measured amount of shocked oxygen of $\sim$0.4 M$_\odot$ (Kosenko et al. 2010) renders this case implausible. According to these plots, our 'merger' model matches the oxygen emissivity of SNR 0519−69.0 for the ISM density range of $(1.5–2.5)\,{\rm cm}^{-3}$. However, at this stage the quality of the data (and the statistical significance of the fit) does not allow us to make a definitive prediction.

7 RESULTS AND DISCUSSION

The method we describe here allows us to constrain the explosion mechanism and progenitor scenario of thermonuclear SNe by investigating emission properties of their remnants. It is based on modelling the soft X-ray spectra produced by the shocked SN ejecta, which can be confronted with the observations of SNRs. This technique can be applied to any remnant of a thermonuclear explosion in order to constrain the nature of its explosion. Comparison of the model spectra with high spectral resolution RGS spectra from two LMC SNRs suggests that a robust identification of the progenitor scenario may be achieved with high-quality data.

Note that for our simulations of the remnant phase we had to use spherically averaged versions of the 3D explosion models described in Section 2, which are generically asymmetric. This may affect the shape and strength of the predicted line features. A proper modelling of the synthetic spectra requires a 3D treatment of the SNR evolution which could be addressed in future studies.

By relating the oxygen emission lines to those of nitrogen we grade most of the uncertainties in the nature of the underlying continuum. The corresponding emission lines lie close to each other in the spectrum and originate from adjacent regions in the shell, however separated by the contact discontinuity. Estimates of the oxygen

[1] Version 12.7.1

[2] The ISM metallicity is 0.3 of solar.

mass in the remnants of SNR 0509−67.5 and SNR 0519−69.0 reported in Kosenko et al. (2008) and Kosenko et al. (2010) are subject to many uncertainties that stem from the poorly known conditions around the SNRs. The robustness of these results should be considered with caution (see the relevant discussions in the aforementioned studies) and they require additional confirmation from other sources and methods. The approach presented here combined with high-quality data has the potential to reconstruct basic properties of the explosion mechanism. The evolutionary plots can serve as a tool for a prompt classification of any SNR with the available soft X-ray data. Observational data points can be straightforwardly derived from the spectra. No complex and cumbersome multicomponent spectral modelling is required.

Our best guess for the ISM density of $\sim$0.5 cm^{-3} for SNR 0509−67.5 agrees with almost all other measurement and with HD models where an explosion of 1.4×10^{51} erg is adopted. Using the presented technique we find that our delayed detonation model (1.4×10^{51} erg, $\sim$0.6 M$_\odot$ of ^{56}Ni) agrees better with the data than the merger for SNR 0509−67.5. However, neither of them is a good model for a 91T-like explosion as inferred for this remnant (Rest et al. 2008; Badenes et al. 2008). The latter is more abundant than 'deldet' in ^{56}Ni ($\sim$1 M$_\odot$), but of the same explosion energy. If that is the case, our comparison with the 'subch' and the 'deldet' models may be significantly affected. For these two models, the amount of oxygen in the ejecta will be significantly lower if the ^{56}Ni mass increases to 1 M$_\odot$. Therefore, it can be seen as an indication in which direction to search for a good model for this particular remnant at best. Once a detailed simulation of SN1991T explosion becomes available it can be applied to SNR 0509−67.5 in this framework.

It is still unclear how the explosion mechanism affects the morphology of SNRs expanding into a uniform medium. SNR 0509−67.5 shows a rather spherical shape (see fig. 1 in Warren & Hughes 2004) which seems natural for single degenerate scenario. For merger remnants in contrast one would expect a more asymmetrical structure. However, a study of Schaefer & Pagnotta (2012) showed no evidence of a surviving companion star in SNR 0509−67.5, challenging an origin from a delayed detonation in a single-degenerate progenitor and indicating a WD merger. As this remnant does not show an oxygen overabundance in its spectra, this could imply an oxygen-poor merger scenario, which could occur if the secondary star is not disrupted, leaving ejecta much more similar to a 'subch' model than our 'merger'. However, in this case there will also be a compact remnant (the secondary WD) left, although very faint and probably undetectable.

In contrast, SNR 0519−69.0 has a tilted axisymmetric morphology (fig. 1 in Kosenko et al. 2010) and our analysis suggests that the most plausible progenitor for this remnant is an oxygen-rich merger. This is in concordance with the high oxygen abundance found by Kosenko et al. (2010) and also in agreement with conclusions of Edwards, Pagnotta & Schaefer (2012) derived from the absence of a companion star in the centre of the SNR. In this scenario, the respective ISM density of $\sim$2.0 cm^{-3} reconciles the X-ray measurements and the HD simulations with explosion energy of 1.6×10^{51} erg. Nevertheless, considerably higher quality of the RGS data is required in order to derive more reliable conclusions on these SNRs.

We note that a SN type Ia progenitor can modify the ambient medium through mass outflow and produce a structured and probably clumpy bubble. This should have noticeable effect on the remnant evolution. Moreover, a wind from a pre-supernova can modify the chemical composition of the circumstellar medium (CSM), which in turn could affect nitrogen abundance and thus its emissivity. Chiotellis et al. (2013) have shown how a non-uniform CSM around a SN progenitor will affect the SNR's evolution and eventually also its X-ray emission. They modelled the remnant of SN 1572 (Tycho) by means of the SUPREMNA code. They also analysed the impact on the X-ray emission from chemically enriched AGB winds, and found that the changes in the integral thermal emission are not noticeable. It is conceivable that in some special cases the nitrogen abundance in the CSM could be modified by the progenitor, thus slightly altering our criteria; however the current accuracy of the measurements would not allow us to distinguish such a minuscule difference.

We note that within the scope of the present paper we focus on the variations caused by different explosion mechanisms only. A more detailed approach would require self-consistent models of stellar evolution and an explosion model coupled to a realistic wind profile. The presence of dense clouds in the vicinity of a supernova could alter the overall properties the remnant's X-ray emission, but in comparison to the effects caused by differences in the chemical composition of the ejecta these effects should be small. In addition, we note that it is commonly assumed that these LMC remnants expand into a uniform medium.

8 CONCLUSION

A method based on state-of-the-art 3D simulations of thermonuclear SN explosions, coupled with hydrodynamic calculations of the SNR's evolution, making use of the most up-to-date atomic data, was used to study the properties of oxygen emission lines in synthetic X-ray spectra. It was shown that confronting these models with observations of young SNRs can help to identify the nature of their progenitors. Our results suggest that for SNR 0519−69.0 an oxygen-rich merger is the preferred scenario whereas SNR 0509−67.5 could be either the result of a delayed-detonation explosion or an oxygen-poor merger. Even though, at present, the quality of data available is insufficient to draw robust conclusions, combining different observations and data allows narrowing down possible scenarios.

ACKNOWLEDGEMENTS

We thank the anonymous referee for useful discussions and comments which considerably helped us to improve the manuscript. DK was supported by RFBR grant 13-02-92119 and by the French national research agency ANR (COSMIS project). She thanks the Max-Planck-Institut für Astrophysik for the warm hospitality. SB was supported by RFBR grant 13-02-92119 and SAI MSU. This work was supported by the Deutsche Forschungsgemeinschaft via the Transregional Collaborative Research Center TRR 33 'The Dark Universe' and the Excellence Cluster EXC153 'Origin and Structure of the Universe'.

REFERENCES

Arnaud K. A., 1996, in Jacoby G. H., Barnes J., eds, ASP Conf. Ser. Vol. 101, Astronomical Data Analysis Software and Systems V, Astron. Soc. Pac., San Francisco, p. 17

Badenes C., Hughes J. P., Cassam-Chenaï G., Bravo E., 2008, ApJ, 680, 1149

Blinnikov S. I., Eastman R., Bartunov O. S., Popolitov V. A., Woosley S. E., 1998, ApJ, 496, 454

Chiotellis A., Kosenko D., Schure K. M., Vink J., Kaastra J. S., 2013, MNRAS, 435, 1659

Ciaraldi-Schoolmann F., Seitenzahl I. R., Röpke F. K., 2013, A&A, 559, A117
den Herder J. W. et al., 2001, A&A, 365, L7
Edwards Z. I., Pagnotta A., Schaefer B. E., 2012, ApJ, 747, L19
Fink M., Hillebrandt W., Röpke F. K., 2007, A&A, 476, 1133
Fink M., Röpke F. K., Hillebrandt W., Seitenzahl I. R., Sim S. A., Kromer M., 2010, A&A, 514, A53
Fink M. et al., 2014, MNRAS, 438, 1762
Ghavamian P., Blair W. P., Sankrit R., Raymond J. C., Hughes J. P., 2007, ApJ, 664, 304
Hillebrandt W., Niemeyer J. C., 2000, ARA&A, 38, 191
Hillebrandt W., Kromer M., Röpke F. K., Ruiter A. J., 2013, Frontiers Phys., 8, 116
Iben I., Jr, Tutukov A. V., 1984, ApJS, 54, 335
Kaastra J. S., Mewe R., Nieuwenhuijzen H., 1996, in Yamashita K., Watanabe T., eds, UV and X-ray Spectroscopy of Astrophysical and Laboratory Plasmas, p. 411. Available at: http://adsabs.harvard.edu/abs/1996uxsa.coll..411K
Kosenko D. I., 2006, MNRAS, 369, 1407
Kosenko D., Vink J., Blinnikov S., Rasmussen A., 2008, A&A, 490, 223
Kosenko D., Helder E. A., Vink J., 2010, A&A, 519, A11
Kosenko D., Blinnikov S. I., Vink J., 2011, A&A, 532, A114
Kosenko D., Ferrand G., Decourchelle A., 2014, MNRAS, 443, 1390
Li W. et al., 2011, MNRAS, 412, 1441
Livne E., 1990, ApJ, 354, L53
Moll R., Woosley S. E., 2013, ApJ, 774, 137
Pakmor R., Kromer M., Taubenberger S., Sim S. A., Röpke F. K., Hillebrandt W., 2012, ApJ, 747, L10
Pakmor R., Kromer M., Taubenberger S., Springel V., 2013, ApJ, 770, L8
Piatti A. E., Geisler D., 2013, AJ, 145, 17
Rest A. et al., 2005, Nature, 438, 1132
Rest A. et al., 2008, ApJ, 680, 1137
Röpke F. K. et al., 2012, ApJ, 750, L19
Schaefer B. E., Pagnotta A., 2012, Nature, 481, 164
Seitenzahl I. R., Meakin C. A., Townsley D. M., Lamb D. Q., Truran J. W., 2009, ApJ, 696, 515
Seitenzahl I. R. et al., 2013, MNRAS, 429, 1156
Shigeyama T., Nomoto K., Yamaoka H., Thielemann F.-K., 1992, ApJ, 386, L13
Sim S. A., Röpke F. K., Hillebrandt W., Kromer M., Pakmor R., Fink M., Ruiter A. J., Seitenzahl I. R., 2010, ApJ, 714, L52
Sorokina E. I., Blinnikov S. I., Kosenko D. I., Lundqvist P., 2004, Astron. Lett., 30, 737
Springel V., 2005, MNRAS, 364, 1105
Vink J., 2012, A&AR, 20, 49
Warren J. S., Hughes J. P., 2004, ApJ, 608, 261
Welty D. E., Frisch P. C., Sonneborn G., York D. G., 1999, ApJ, 512, 636
Whelan J., Iben I., Jr, 1973, ApJ, 186, 1007

This paper has been typeset from a TEX/LATEX file prepared by the author.